Available online at www.sciencedirect.com
SCIENCE DIRECT®
International Journal of Heat and Fluid Flow 24 (2003) 596–605
International Journal of HEAT AND FLUID FLOW
www.elsevier.com/locate/ijhff

Large eddy simulation of vortex breakdown behind a delta wing

I. Mary *

ONERA, 29 Avenue de la Division Leclerc, 92322 Châtillon cedex, France

Received 22 November 2002; accepted 15 March 2003

Abstract

A large eddy simulation (LES) of a turbulent flow past a 70° sweep angle delta wing is performed and compared with wind tunnel experiments. The angle of attack and the Reynolds number based on the root chord are equal to 27° and 1.6×10^6, respectively. Due to the high value of the Reynolds number and the three-dimensional geometry, the mesh resolution usually required by LES cannot be reached. Therefore a local mesh refinement technique based on semi-structured grids is proposed, whereas different wall functions are assessed in this paper. The goal is to evaluate if these techniques are sufficient to provide an accurate solution of such flow on available supercomputers. An implicit Miles model is retained for the subgrid scale (SGS) modelling because the resolution is too coarse to take advantage of more sophisticated SGS models. The solution sensitivity to grid refinement in the streamwise and wall normal direction is investigated.

Keywords: LES; Delta wing; Vortex breakdown; Local mesh refinement; Semi-structured grids; Wall function

1. Introduction

The need to improve fighter aircraft maneuverability has inspired extensive study of the flow past delta wings. At high angle of attacks, complex three-dimensional separated flowfields are present on the suction side of the wing. The most prominent vortical structures are the leading edge vortices, which are subjected to a sudden disorganization when the angle of attack becomes sufficiently high. This phenomenon, known as vortex breakdown and characterized by a severe decrease of the lift coefficient, often limits the aircraft flight capacity. Thus, for several decades, numerous analytical and experimental studies have been dedicated to the characterization of this vortex breakdown and to the study of its control (see Werlé, 1960; Leibovitch, 1978, for instance).

The global vortex breakdown properties are now relatively well understood, but their control still remains a challenging task. Recently, control devices based on oscillatory flow excitations have been investigated by different researchers as a means to delay the onset of vortex breakdown (see Guy et al., 2000; Mitchell et al., 2000a, for instance). As this control strategy involves the introduction of small time-dependent perturbations near the leading edge, large eddy simulation (LES) appears to be a potential numerical tool to achieve further insights in the control mechanism.

However the high value of the Reynolds number and the three-dimensional geometry do not allow the mesh resolution usually required by LES of wall bounded flow ($\Delta y^+ \leqslant 2$, $\Delta z^+ \approx 20$, $\Delta x^+ \approx 100$) to be handled. Therefore, such computations must be assessed in order to determine their reliability. Indeed, recent studies dealing with complex flows around airfoils have shown the current limits of this approach, since LES results obtained on coarse grids were often worse than URANS (Davidson et al., 2003). These results however concern an almost attached flow and the conclusions could be rather different for a massively separated flow, like the vortex breakdown considered here. The reason is that the flow dynamics may be mainly governed by the large separated scale, and not by the near wall turbulent vortical structures, such as streaks. For instance, recent computations of flow over an open cavity have demonstrated that LES can provide very accurate solutions even on coarse grids (Larchevêque et al., 2003). However for the flow past a delta wing, the coupling between the small and large scale vortices associated with the

* Fax: +33-1-4673-4166.
E-mail address: imary@onera.fr (I. Mary).

0142-727X/03/$ - see front matter © 2003 Elsevier Science Inc. All rights reserved.
doi:10.1016/S0142-727X(03)00053-5

suction side boundary layer and the leading edge respectively, could be strong enough to require an appropriate resolution of the smallest eddies. The focus of this paper is therefore to examine this coupling intensity, and consequently to evaluate the reliability of LES on coarse grid for this type of flow. As the physics of the non-controlled flow appear sufficiently challenging for LES, this simpler case has been retained for the assessment. Different numerical techniques, ranging from wall functions to a local mesh refinement, have been investigated in a finite-volume structured solver in order to evaluate their abilities to minimize the errors related to the grid resolution. The wall functions, which can allow a coarser resolution for some academic flow cases (Nicoud et al., 2001), seem to be quite inefficient for complex flows containing separation zones (Davidson et al., 2003). Therefore the accuracy of this approach generally depends on the flow case considered. For the delta wing flow case, it seems that no wall function assessment is referenced in the literature. Therefore a classical logarithmic law and a slip condition have been evaluated at the wall, in order to determine their accuracy for the considered flow case and for a mesh resolution given by the current limitation of available supercomputers.

The second way explored to limit the computational cost of LES relies on a local mesh refinement. This technique reduces the required number of grid points for a simulation by adapting the mesh resolution to the local flow length scales. Unstructured meshes are a natural tool to achieve an efficient cells distribution. Due to their cost and to the difficulty to achieve high order of accuracy, however they have not yet been applied to DNS and LES very extensively. For structured solvers, several techniques based on semi-structured meshes have been recently used by different researchers. For instance computations of a flow around an airfoil (Mary and Sagaut, 2002; Schmidt et al., 2001) have shown that a local mesh refinement technique could be a promising tool to handle LES of complex flows. Nevertheless, for the flow past a delta wing, the interface between non-coincident blocks should be located in a turbulent zone to achieve a decrease in the total number of points, thus requiring a more accurate treatment of the block interface problem. For the case of turbulent channel flow, Quéméré et al. (2001) have shown that the different cut-off lengths associated with each semi-structured block necessitate the use of an enrichment procedure to preserve the simulation accuracy in the fine block. This technique, which leads to impose discontinuous unsteady flow variables values at the interface, has been developed for cartesian grid. Therefore its application to the present complex case should provide further validations in terms of accuracy and robustness.

The governing equations are presented in Section 2, whereas the numerical method is described in Section 3. Section 4 is devoted to the presentation of the test case and the results comparison.

2. Governing equations and SGS model

A dimensionless form of the three-dimensional unsteady filtered Navier–Stokes equations are used for a viscous compressible Newtonian fluid. Any flow variable ϕ can be written as $\phi = \bar{\phi} + \phi'$, where $\bar{\phi}$ represents the large scale part of the variable and ϕ' its small scale part. The filtering operator, classically defined as a convolution product on the computational domain, is assumed to commute with time and spatial derivatives. Moreover, for the clarity of the equations it is convenient to introduce the Favre filtering, defined by $\tilde{\phi} = \overline{\rho\phi}/\bar{\rho}$. In conservative form, the filtered Navier–Stokes equations can be expressed in three-dimensional cartesian coordinates (x_1, x_2, x_3) as:

$$\frac{\partial \overline{Q}}{\partial t} + \frac{\partial \overline{F}_j}{\partial x_j} - \frac{1}{Re}\frac{\partial \overline{F}_j^{\mathrm{v}}}{\partial x_j} = S \tag{1}$$

The symbol S, which denotes the subgrid scale (SGS) contribution, is fully described by Lenormand et al. (2000), whereas the Reynolds number is defined by $Re = \rho_0 u_0 L_0/\mu_0$. The symbols u_0, ρ_0, L_0 and μ_0 denote the characteristic velocity, density, length and dynamic viscosity, respectively. The conservative flow variables, $\overline{Q}$, the inviscid fluxes, $\overline{F}_j$, and the viscous fluxes, $\overline{F}_j^{\mathrm{v}}$, are defined by:

$$\begin{aligned}
\overline{Q} &= \left(\bar{\rho}, \bar{\rho}\tilde{u}_1, \bar{\rho}\tilde{u}_2, \bar{\rho}\tilde{u}_3, \frac{\bar{p}}{\gamma-1} + \frac{\bar{\rho}\tilde{u}_j\tilde{u}_j}{2}\right)^{\mathrm{t}} \\
\overline{F}_j &= \tilde{u}_j\overline{Q} + \left(0, \delta_{1j}\bar{p}, \delta_{2j}\bar{p}, \delta_{3j}\bar{p}, \bar{p}\tilde{u}_j\right)^{\mathrm{t}} \\
\overline{F}_j^{\mathrm{v}} &= \mu\left(0, \widetilde{S}_{1j}, \widetilde{S}_{2j}, \widetilde{S}_{3j}, \widetilde{S}_{kj}\tilde{u}_k + \frac{1}{P_r}\frac{\partial \widetilde{T}}{\partial x_j}\right)^{\mathrm{t}} \\
\widetilde{S}_{ij} &= \frac{\partial \tilde{u}_i}{\partial x_j} + \frac{\partial \tilde{u}_j}{\partial x_i} - \frac{2}{3}\delta_{ij}\frac{\partial \tilde{u}_k}{\partial x_k}
\end{aligned} \tag{2}$$

These equations are supplemented with the filtered equation of state, $\bar{p} = \bar{\rho}\widetilde{T}/(\gamma M_0^2)$, where M_0 represents a reference Mach number. To obtain a correct dissipation rate, all classical SGS models require the cut-off length of the mesh to be located in the inertial range of turbulent kinetic energy (TKE) spectrum. Such a fine mesh is not affordable in the present case due to the high value of the Reynolds number. As a consequence the simulations have been carried out with the Miles approach (Boris et al., 1992), in which the SGS term in Eq. (1) is set to zero. In this case an energy transfer from the large scales to the small ones is achieved by the use of a dissipative scheme for the discretization of the convective fluxes. This technique must be used with some cautions, since the result can be influenced by the choice of both

the dissipative scheme used to discretize the Euler fluxes and the mesh resolution. However it has been shown that this approach can give satisfactory results as long as the driving mechanism of the flow is well discretized. This model has been successfully validated for a spanwise homogeneous flow past a deep cavity, when the global dynamics is governed by large scale vortices (Larchevêque et al., 2003). When the dynamics is mainly governed by the small scale vortices of a spanwise homogeneous boundary layer, the Miles model is slightly less accurate than an explicit SGS model (Mary and Sagaut, 2002) if the cut-off length of the mesh is located in the inertial range of the TKE spectrum. Otherwise Miles and all classical explicit SGS models lead to rather unaccurate prediction of boundary layers. Due to the high value of the Reynolds number in the present case, a correct discretization of the boundary layer is not affordable. Therefore the simple Miles model is retained and wall functions will be used to improve the results in the boundary layers. It must be mentioned that explicit mixed scales model (Lenormand et al., 2000) has been used in a previous simulation of the same configuration and with the same wall functions. The results were very similar to those obtained with the Miles (Leroy and Mary, 2001).

3. Numerical method

3.1. General description

The Navier–Stokes equations are discretized using a cell-centered finite volume technique and structured multi-block meshes. The Euler fluxes are discretized by a modified AUSM+(P) upwind scheme (Mary and Sagaut, 2002), whereas a second-order accurate centered scheme is used for the viscous fluxes. For a reason of efficiency, a second-order accurate implicit time integration is employed to deal with the very small grid size encountered near the wall. An approximate Newton method is used to solve the non-linear problem. At each iteration of this inner process, the inversion of the linear system relies on lower–upper symmetric gauss-seidel (LU-SGS) implicit method. More details about these numerical points are available in Péchier et al. (2001).

3.2. Wall function

A large variety of phenomena occurs in the boundary layers (BL). On the pressure side the BL remains very thin and laminar, whereas the BL becomes turbulent on the suction side, with separation near the leading edge. A crude extrapolation of a recent European study conclusion (Davidson et al., 2003) shows that nearly 60×10^6 cells should be necessary just to well resolve the near wall region of the suction side. Since such grid is not affordable, wall functions have been used in an attempt to "model" the effect of the near wall turbulent structures, which cannot be represented by the grid. However the accuracy of this approach is not really established for LES especially for complex flows, despite the different works dedicated to this topic during the last decades (see Nicoud et al., 2001, for a review). Therefore two approximate boundary conditions have been assessed in order to determine their accuracy for the current flow case.

The first wall function is based on a no-slip condition and the shear stress in adjacent cells to a wall, τ_p, is obtained from an analytical velocity profile thanks to a Newton process:

$$\begin{aligned} \tau_p &= \rho u_\tau^2 \\ u^+ &= \frac{u}{u_\tau} = f\left(\frac{y u_\tau}{\nu_p}\right) = f(y^+) \\ &= \begin{cases} y^+ & \text{if } y^+ < 11,\ 13 \\ 0.41^{-1}\ln y^+ + 5,\ 25 & \text{if } y^+ > 11,\ 13 \end{cases} \end{aligned} \tag{3}$$

where u_τ, y and ν_p represents the friction velocity, the distance to the wall and the viscosity at the wall, respectively. To compute boundary layer separation, the wall law is expressed in a reference frame defined by the velocity direction in adjacent cells to a wall (see Goncalves and Houdeville, 2001, for more details).

The second wall function is very crude, since a slip condition is applied at the wall and the wall shear stress is set to zero.

3.3. Local mesh refinement technique

The grid generation constitutes a big issue for this flow case. Indeed the center of the leading edge vortices is quite far from the boundary layer of the suction side wall because of the high angle of attack. As it appears reasonable to locate at least 20–30 cells in the core of the leading edge vortices, a fine resolution must be kept in the wall normal direction up to 30% of the root chord. Therefore the mesh size can become prohibitive, since this dense resolution must be kept in the far-field and in the wake with a structured solver. Thus, a local mesh refinement technique is retained in order to concentrate a large majority of the cells in the zone located above the suction side. The method is based on the use of different blocks characterized by a cell face ratio larger than one at the interface. Hence the information transfer between coarse and fine block, which is realized through ghost cells, constitutes the main difficulty of this approach. In order to illustrate the numerical problem, Fig. 1(a) shows a schematic representation of the blocks interface for a simple two-dimensional case. Following the work of Quéméré et al. (2001), the discontinuity in the characteristic lengths along the domain interface Γ involves a discontinuity in the spectral representation of the

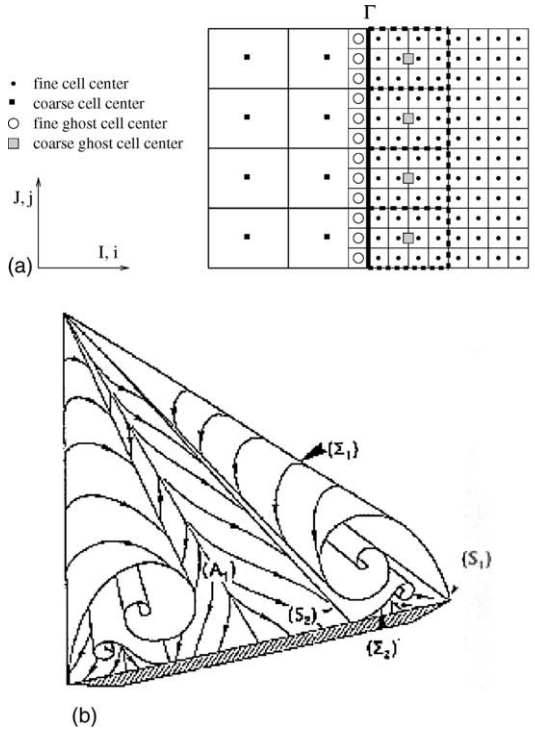

Fig. 1. (a) Representation of the block interface, (b) flowfield topology (Mitchell et al., 2000a).

flowfield. Therefore a frequential restriction procedure is needed to transfer informations from the fine mesh resolution to the coarse one, whereas a frequential enrichment procedure is used to determine the value of the fine ghost cells from solution on the low-level resolution grid.

3.3.1. Restriction procedure

The information transfer between the fine grid solution and the coarse grid solution (noted Q_f and Q_c respectively) is realized by applying a low-past filter to Q_f. This low-past filter is based on a simple volumic average and leads to the following definition of Q_c^{ghost} in the ghost cells:

$$Q_c^{ghost}(J) = \frac{1}{\Omega_c}\int_{\Omega_c} Q_f \, dv \tag{4}$$

where Ω_c represents the volume delimited by the dashed line on Fig. 1(a).

3.3.2. Enrichment procedure

The basic idea of this procedure is to furnish from the coarse solution Q_c a data which contains a spectral information close to the solution on the fine block Q_f. Following Quéméré et al. (2001), these high frequencies are regenerated from the informations contained in the fine-resolution subdomain. The first step of this procedure consists in defining a low-resolution field at each cell of the fine mesh located in the ghost and the first current rows (noted $\overline{Q}_f^0$ and $\overline{Q}_f^1$ respectively). This is achieved by using a second-order accurate three-linear interpolation operator L_{xyz}:

$$\begin{aligned}\overline{Q}_f^0 &= L_{xyz}\left(Q_c, Q_c^{ghost}, i=0\right)\\ \overline{Q}_f^1 &= L_{xyz}\left(Q_c, Q_c^{ghost}, i=1\right)\end{aligned} \tag{5}$$

This operator, which is different from the third-order accurate one of Quéméré et al. (2001) developed for uniform cartesian grid, is chosen because it is very difficult to achieve such order of accuracy on arbitrary curvilinear grid. In addition it is much more efficient, since only 8 nodes for a three-dimensional case (instead of 27) are required to compute $\overline{Q}_f$. Finally a first order extrapolation is used to regenerate the high frequencies information in the ghost cells from Q_f. This leads to the following definition of Q_f^{ghost}:

$$Q_f^{ghost}(j) = \overline{Q}_f^0(j) + C\left(Q_f^1(j) - \overline{Q}_f^1(j)\right) \tag{6}$$

where Q_f^1 represents the value of Q_f in the first current row of the fine grid and C is a binary enrichment coefficient. Indeed due to the lack of accuracy of the three-linear interpolation operator L_{xyz}, the frequency complement (corresponding to the second term in Eq. (6)) can be slightly different from zero even if the flow is laminar. Thus, in order to prevent a possible spurious transition process to turbulence the value of C is set to zero if the block interface is located in a laminar zone. Otherwise this value is equal to 1. The drawback of this simple strategy is that the block interface cannot be located in a transitional zone. However this constraint is not very prejudicious. Indeed, the frequency complement definition renders necessary to locate a low-resolution domain downstream of a turbulence production zone, which constitutes clearly the most limiting constraint for the grid generation. Otherwise Q_f is not able to provide a reliable frequency complement, and the usual problem of inflow condition for LES arises (Batten et al., 2001).

4. Numerical results

4.1. Test case

A 70° sweep angle delta wing with sharp leading-edges has been chosen for the study, because the detailed experimental data of Mitchell et al. (2000b) are available. The flow configuration is quite realistic: the Reynolds number, based on the root chord ($c = 0.95$ m), and the upstream velocity ($u_\infty = 24\ \mathrm{m\,s^{-1}}$), is equal to 1.6×10^6, whereas the angle of attack is set to 27°. The model has a wingspan of 0.69 m at its trailing edge, is 0.02 m thick, and is beveled on the windward side at an angle of 15° to form sharp leading edges. Fig. 1(b) is a schematic portrayal of the flow topology, which clearly distinguishes the main leading-edge (Σ_1) and the

secondary (Σ_2) vortices. The main detachment should be quite well represented by LES due to the sharp leading edges. But it seems much more difficult to obtain a correct representation of the secondary one, because it should be strongly influenced by the near-wall resolution and the wall function.

4.2. Computational setup

Three different meshes composed of 14 blocks have been used to investigate the simulation sensitivity to some spatial resolution parameters. As a previous study (Leroy and Mary, 2001) has shown that the use of a symmetry condition does not affect the simulation accuracy, only one half of the model is discretized. The limits of the computational domain are located at about 10 chords of the wing, whereas the general mesh topology is illustrated on Fig. 2. The view of the plane of symmetry shows that the origin is set at the apex of the wing, whereas the trailing edge (TE) is located at $x/c = 1$. The thick line, which indicates the interface between fine and coarse resolution subdomains, shows that the far-field and the wake are discretized with coarse grids. The N_i rows of Table 1, which are associated with the fine domain discretizing the leading-edge (LE) vortex, indicate approximately the number of cells

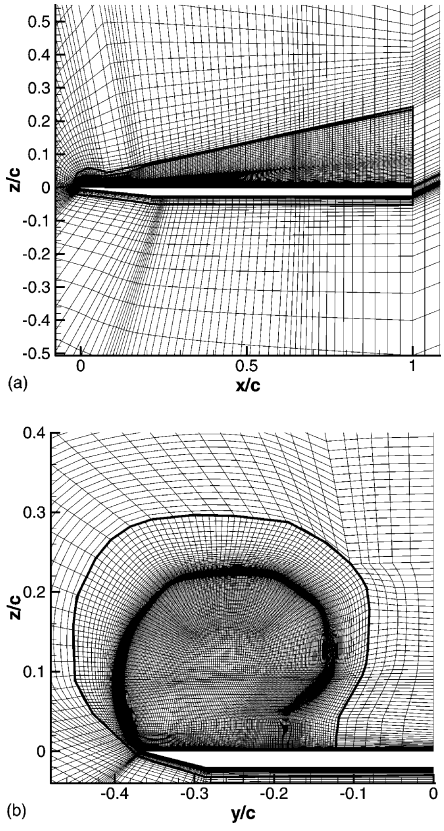

Fig. 2. View of M_1 mesh: (a) plane of symmetry and (b) trailing edge plane.

in the streamwise, wall normal and spanwise directions respectively. The enrichment procedure is used at the TE block interface ($x/c = 1$) located in the (y,z) plane (see Fig. 2(b)). The cell face ratio is given in Table 1 by $\mathrm{TE}_{\mathrm{ratio}}$. For instance 6/3/3 indicates that the resolution of the domain located in the wake of the fine subdomain is three time coarser in the y and z directions and 6 times coarser in the streamwise direction. It has been shown in Leroy and Mary (2001) for vortex advection test cases that the local grid refinement technique is able to give accurate results for such mesh discontinuity. The row $N_{\mathrm{b.pts}}$ corresponds to the total number of cells, whereas the mesh resolution in the direction normal to the suction side of the wing is given by Δz_{wall}. The M_k grids ($k = 1, 3$) only differ by mesh characteristics of the fine block delimited by the thick line. On the one hand, the M_1 and M_2 meshes are used to evaluate the capability of the wall functions presented above. Indeed these grids have the same resolution in the wall normal direction ($\Delta z_{\mathrm{wall}} = 60$–$100$ μm). In term of wall units, this resolution corresponds to $\Delta z^+ = 20$–30. These numbers are meant to convey the general order of magnitude rather than the precise values. The difference between the M_1 and M_2 meshes concerns the streamwise resolution, which is two times finer on the M_2 grid ($\Delta x^+ = 70$–700). On the other hand, the M_3 grid is designed to obtain a correct discretization of the mean flowfield in the (y,z) plane. At the wall the mesh size is around one order of magnitude smaller ($\Delta z^+ \approx 2$) than in the M_1 and M_2 meshes. Moreover the grid resolution in the vortex sheet, associated with the LE vortex, has been improved to. A posteriori analysis shows that around 30 cells are located in the suction side boundary layer, in the vortex sheet near the LE and in the vortex core. Despite these improvements of the mesh resolution, no reference solution can be obtained on this M_3 grid, since the streamwise resolution is identical to those of the M_1 grid. This M_3 mesh is only used to evaluate for the present test case the accuracy of a LES performed on a mesh, which is adapted to a RANS simulation without wall function. Therefore a usual no-slip condition will be used at the wall with this M_3 grid. A uniform flowfield is retained as initial condition. The time step is fixed at $\Delta t = 3.5 \times 10^{-5} c/u_\infty$ implying a maximal CFL number close to 16. Around 8 time units are necessary to evacuate from the flowfield the errors related to the initial uniform solution. For average quantities, the averaging procedure is performed in time over a period of $2.4c/u_\infty$. As the turbulent vortices have a characteristic time shorter than $0.1c/u_\infty$ (Molton et al., 1999), this time integration appears generally sufficient to converge the average quantities. However in the vicinity of the vortex breakdown position, the flow is subjected to a low frequency flapping ($f \approx u_\infty/c$) in the streamwise direction. Therefore the mean flow should be analyzed with some cautions near the breakdown position. The simulations are

Table 1
Mesh characteristics

Mesh	N_1	N_2	N_3	TE_{ratio}	Δz_{wall} (μm)	Δz^+_{wall}	$N_{b.pts}$
M_1	120	120	100	3/3/3	60–100	20–30	1.9×10^6
M_2	240	120	100	6/3/3	60–100	20–30	3.8×10^6
M_3	120	160	140	3/3/3	5–10	2–3	3.5×10^6

carried out on a single processor of NEC SX5 with a well vectorized solver (4Gflops). Almost 190 CPU hours are needed to performed the time integration over this period of $2.4c/u_\infty$ on the largest grid M_3.

4.3. Results discussion

4.3.1. Instantaneous flowfield

The plane of symmetry is used to rebuilt the entire flowfield in order to achieve a better visualization. Fig. 3, which depicts some views of a Q-criterion isosurface (second invariant of $\underline{\underline{\nabla}}\mathbf{u}$), highlights the influence of the suction side boundary condition on the flow structures. With a slip condition, the LE vortex remains well organized up to a position which slightly fluctuates around $x/c = 0.7$. After this point the vortex breakdown occurs and smaller turbulent vortices are generated. If the logarithmic law condition is used, the flow structures are quite different. On the one hand a kind of Kelvin–Helmholtz instability generated at the LE turns around the core of the prominent LE vortex. The burst of this vortex is not significantly influenced by these secondary vortices, which are mixed with the vortices generated by the burst downstream $x/c = 0.7$. On the other hand, coherent elongated structures are present in the boundary layer near the LE, but their reliability in terms of size and intensity is questionable due to the mesh resolution unadapted to these near wall structures. In the wake the mesh resolution of the coarse block does not allow these small structures to be represented. But their size in the fine block, which seems to be nearly constant from the burst position to the TE plane, suggests that the enrichment procedure based on the Eq. (6) works well. Otherwise the size of the vortices should increase significantly in the fine block in the vicinity of the trailing edge interface. In order to illustrate its behavior, a sampling of the velocity magnitude has been recorded in the core of the vortex at the TE block interface. Fig. 4(a) shows the time history of the values associated with the fine and coarse ghost cells, which determine the coupling between the fine solution above the suction side and the coarse one in the wake. As expected the signal recorded on the fine domain clearly

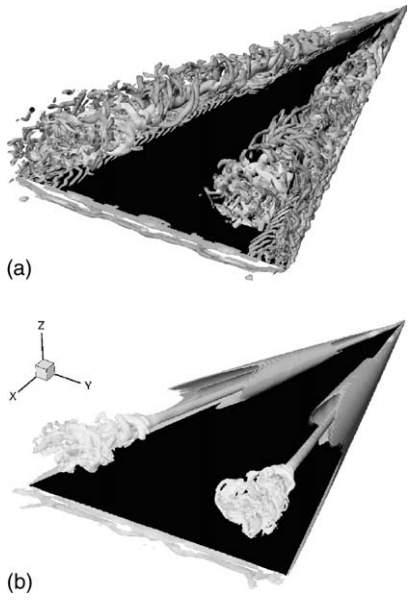

Fig. 3. Q-criterion isosurface: (a) M_2, log and (b) M_2, slip.

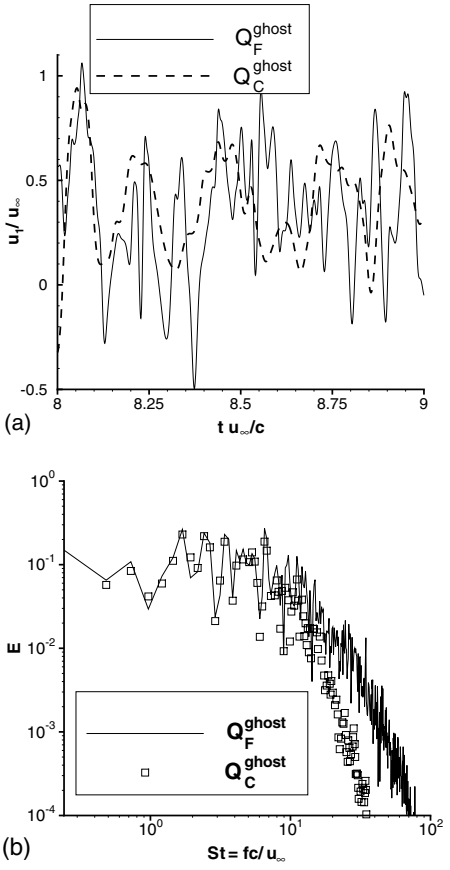

Fig. 4. Analysis of the velocity magnitude signal at $(x/c, y/c, z/c) = (1, -0.24, 0.12)$ (M_2, log).

contains higher frequencies than those recorded on the low-resolution domain. Fig. 4(b), which gives an energy spectrum, allows the frequential information of the two signals to be quantified. It appears that up to a Strouhal number equals to 10 no significant differences occur, whereas the energy contained in higher frequencies are less important on the coarse grid.

4.3.2. Mean flowfield

Some profiles of both the velocity magnitude and the TKE are compared with the experimental measurements in Figs. 5 and 6. These profiles are extracted at two different stations ($x/c = 0.5$ and 0.7) in order to characterize the solution upstream and downstream of the vortex breakdown, respectively. In the same way three

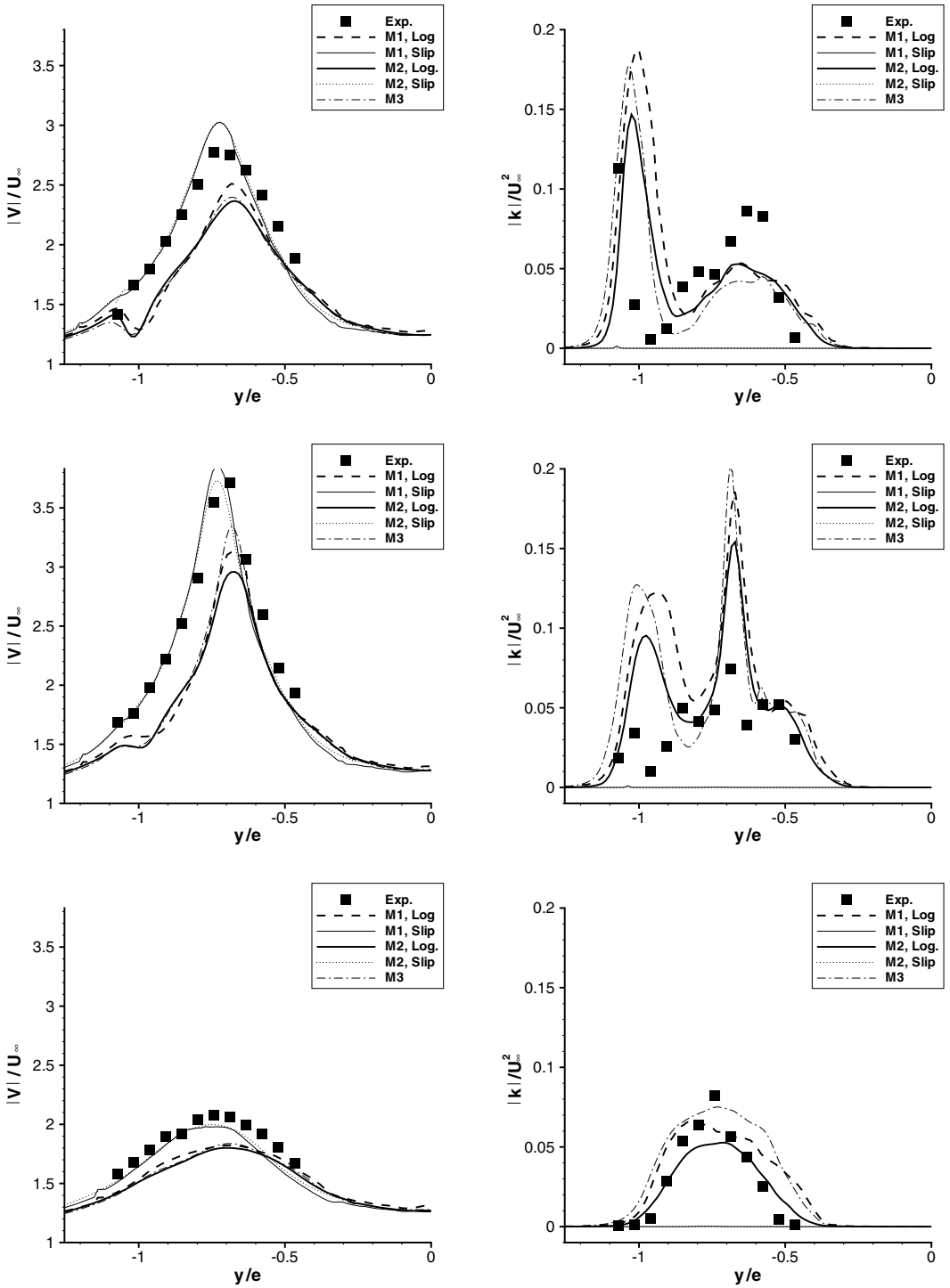

Fig. 5. Profiles of the velocity magnitude and TKE at $x/c = 0.5$: $z/c = 0.04$ (top), $z/c = 0.07$ (center) and $z/c = 0.1$ (bottom).

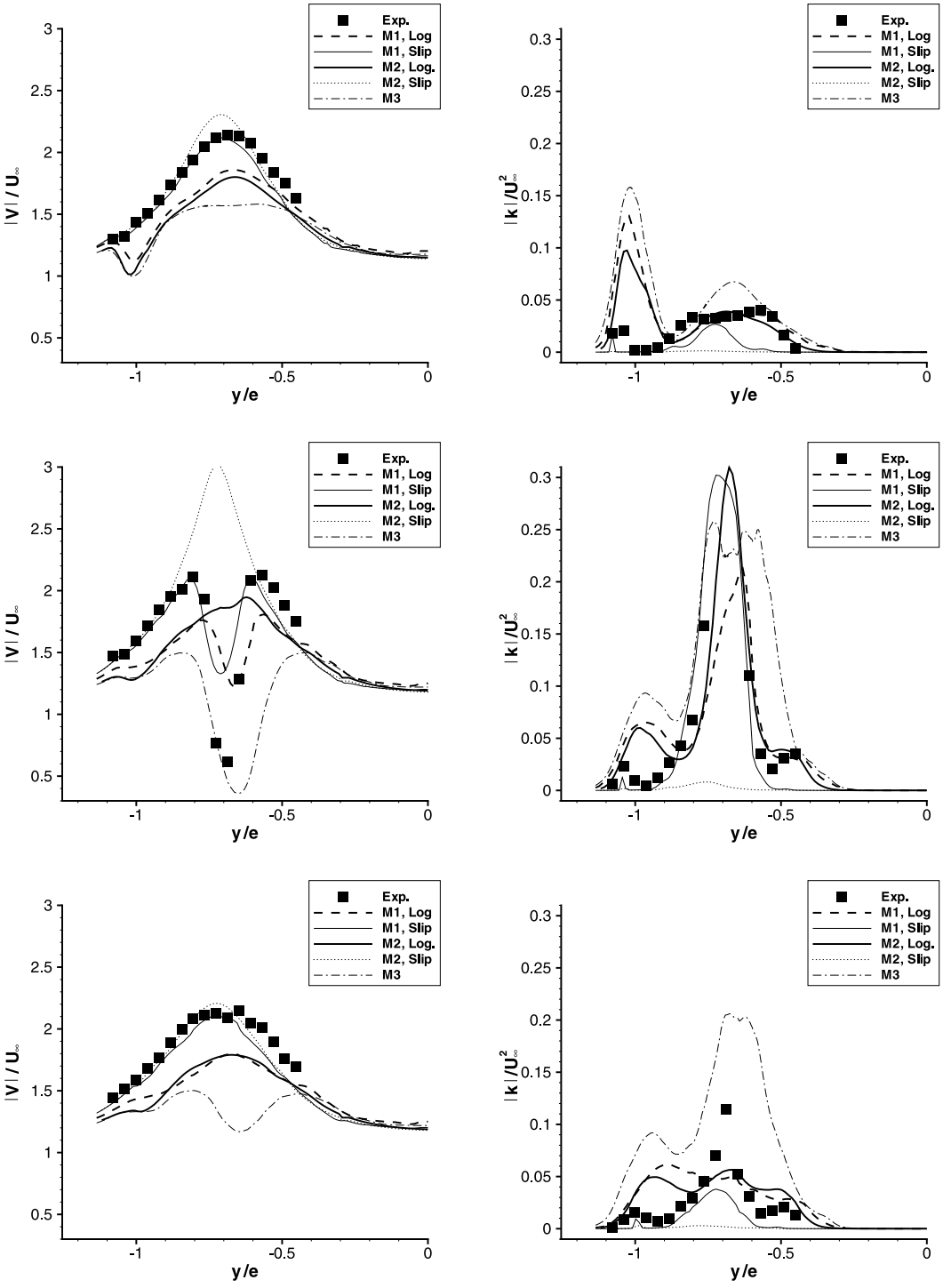

Fig. 6. Profiles of the velocity magnitude and TKE at $x/c = 0.7$: $z/c = 0.05$ (top), $z/c = 0.1$ (center) and $z/c = 0.12$ (bottom).

different distances from the wall have been considered to explore some zones in the vicinity of the LE vortex: one located between the vortex and the wall, one in the core of the vortex and one in the region above. Thus, the profiles are function of the y coordinate normalized by the wingspan at the considered x/c station, e. Therefore $y/e = 0$ and $y/e = -1$ correspond to the plane of symmetry and the leading edge, respectively. The analysis of Fig. 5 clearly demonstrates that the boundary condition used at the wall has more influence on the solution accuracy than the effect due to the different mesh resolution employed in this study. Indeed, all simulations carried out with the Log law wall model exhibit the same behavior. The velocity magnitudes in the core of the

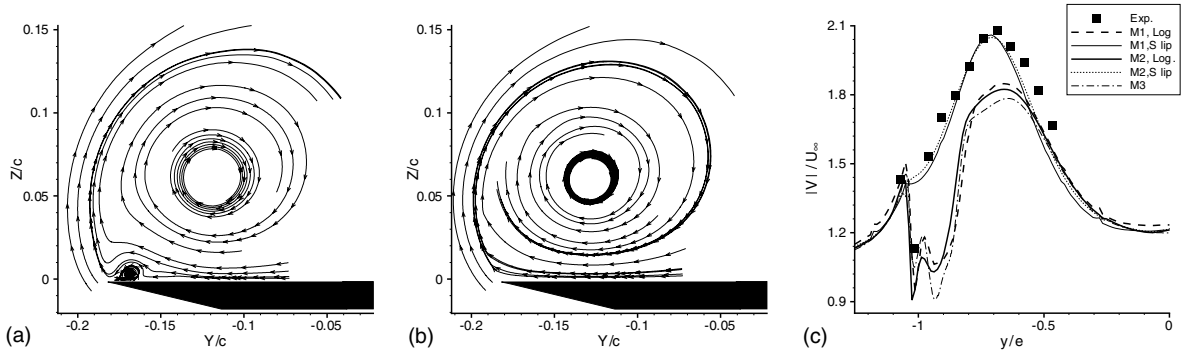

Fig. 7. Suction side boundary layer at $x/c = 0.5$. (a) Streamlines M_2, log. (b) Streamlines M_2, slip. (c) Profiles of velocity magnitude at $z/c = 0.01$.

vortex and near the leading edge are strongly underpredicted before the breakdown. Downstream of $x/c = 0.5$, these errors are propagated and no simulation is able to predict accurately the solution after the breakdown position. Surprisingly, the simulations carried out with a slip condition are much more accurate. Before the breakdown ($x/c = 0.5$) the results obtained on the M_1 and M_2 meshes are both very close to the experimental profiles, showing that the streamwise mesh resolution plays a little role at this station. This is no longer true after this position. Indeed the use of the finest streamwise resolution (M_2) delays the breakdown, which occurs around $x/c = 0.78$ instead of $x/c = 0.69$ with M_1, whereas this phenomenon is located around 0.66 in the experiment. One possible explanation is that for the M_1 simulation, the errors due to the approximate boundary condition counterbalance some discretization errors, leading to a quite satisfactory solution upstream and downstream of the breakdown. The solution obtained on the M_3 grid with usual no-slip condition is quite similar to those obtained with the Log-law on the M_1 and M_2 meshes. Indeed the improvement related to this simulation only concerns the undershoot of the velocity in the core of the vortex upstream of the breakdown position. Moreover this phenomenon occurs slightly too early with this simulation (around $x/c = 0.6$). Concerning the TKE profiles, several remarks can be done. On the one hand, the simulations carried out with the slip condition predict that the flow remains almost steady and laminar up to the breakdown position. This behavior is very different from those observed in the experiment, where significant velocity fluctuations were recorded at $x/c = 0.5$. On the other hand, the simulations carried out with Log-law condition or on the M_3 grid strongly overestimate the peak associated with the vortex sheet around $y/e = -1$. The secondary detachment Σ_2 (see Fig. 1(b)) in the suction side boundary layer is the principle origin of the difference between solutions obtained with slip and no-slip condition. Fig. 7(a) and (b) represents the streamlines of the solutions computed on the M_2 grid with the different wall functions in the (y, z) plane at $x/c = 0.5$. This shows that the use of non-slip condition leads to a small detachment near the leading edge. However this phenomenon is not quantitatively well-predicted, as shown by the velocity profile presented in Fig. 7(c). If the sudden decrease of the velocity is quite well-predicted around the leading-edge at $y/e = -1$, the rapid flow acceleration observed in the experiment when y/e increases is not recovered by the simulation, leading to a poor prediction of the velocity profile. The same analysis can be done with the result obtained on the M_3 grid. Thus, it appears that the size of the separation zone is strongly overpredicted by the simulation using a no-slip condition. Surprisingly the use of a slip condition leads to much better results quantitatively, despite no separation occurs in these simulations.

5. Conclusions and perspectives

A LES of a turbulent flow past a 70° sweep angle delta wing has been performed and compared with wind tunnel experiments for a Reynolds number equal to 1.6×10^6. If the local mesh refinement technique proposed is reasonably well working for this complex case, the use of a no-slip condition with or without wall function based on logarithmic law cannot be recommended. Indeed, all simulations carried out with such boundary condition lead to rather inaccurate results, despite some grid refinements in the streamwise and wall normal direction have been investigated. If quite satisfying results have been obtained with the use of a slip condition at the wall, such strategy does not allow a correct solution near the leading edge to be represented. As most of the attempts to control the vortex breakdown are based on the introduction of some flow perturbations near the leading edge, it appears that LES is not able to give a correct solution of this complex flow with the present meshes. Therefore a much finer grid should be used to simulate accurately with LES the problem of transition and turbulent separation which occur on the suction side. With the grids employed in this work, the use of some hybrid RANS/LES method could lead to a

better description of the suction side boundary layer. But it requires a RANS model able to treat accurately both transition and separation phenomena.

References

Batten, P., Goldberg, U.C., Palaniswamy, S., Chakravarthy, S.R., 2001. Hybrid RANS/LES: spatial-resolution and energy-transfer issues. In: Turbulent and Shear Flow Phenomena 2nd International Symposium, Stockolm, Sweden.

Boris, J.P., Grinstein, F.F., Oran, E.S., Kolbe, R.L., 1992. New insights into large eddy simulation. Fluid Dynam. Res. 10, 199–228.

Davidson L., Cokljat D., Fröhlich J., Leschziner M., Mellen C., Rodi W. (Eds.), 2003. LESFOIL: LES of Flow Around a High Lift Airfoil. Notes on Numerical Fluid Mechanics, Vol. 83. Springer.

Goncalves, E., Houdeville, R., 2001. Reassessment of the wall functions approach for RANS computations. Aerosp. Sci. Technol. 5, 1–14.

Guy, Y., Morrow, J.A., McLaughlin, T.A., Wygnanski, I., 2000. Parametric investigation of the effect of active control of the normal force on a delta wing. AIAA Paper 2000-0550.

Larchevêque, L., Sagaut, P., Mary, I., Labbé, O., Comte, P., 2003. LES of a compressible flow past a deep cavity. Phys. Fluid 15, 193–210.

Leibovitch, S., 1978. The structure of vortex breakdown. Ann. Rev. Fluid Mech. 10, 221–246.

Lenormand, E., Sagaut, P., Ta Phuoc, L., 2000. Large-eddy simulation of subsonic and supersonic channel flow at moderate Reynolds number. Int. J. Numer. Meth. Fluids 32, 369–406.

Leroy, G., Mary, I., 2001. PEA aérodynamique et mécanique du vol: Prédiction de l'éclatement tourbillonnaire sur une aile delta par la SGE. Rapport ONERA, RA 8/05284 DSNA.

Mary, I., Sagaut, P., 2002. LES of flow around an airfoil near stall. AIAA J. 40, 1139–1145.

Mitchell, A., Molton, P., Barberis, D., Gobert, J.L., 2000a. Control of vortex breakdown by along-the-core blowing. AIAA Paper 2000-2608.

Mitchell, A., Molton, P., Barberis, D., Délery, J., 2000b. Characterization of vortex breakdown by flow field and surface measurements. AIAA Paper 2000-0788.

Molton, P., Barberis, D., Mitchell, A., 1999. Etude expérimentale de l'éclatement tourbillonnaire sur une aile delta de 70 degrés de flèche en écoulement incompressible. Analyse des répartitions de la pression pariétale. Rapport ONERA, RT 124/7078 DAFE/N.

Nicoud, F., Bagett, J.S., Moin, P., Cabot, W., 2001. LES wall-modelling based on suboptimal control theory and linear stochastic estimation. Phys. Fluids 13, 2968–2984.

Péchier, M., Guillen, P., Gayzac, R., 2001. Magnus effect over finned projectiles. J. Spacecraft Rockets 38, 542–549.

Quéméré, P., Sagaut, P., Couailler, V., 2001. A new multi-domain/multi-resolution method for large eddy simulation. Int. J. Numer. Meth. Fluids 36, 391–416.

Schmidt, S., Franke, M., Thiele, F., 2001. Assessment of SGS models in LES applied to a naca 4412 airfoil. AIAA Paper 2001-0434.

Werlé, H., 1960. Sur l'éclatement des tourbillons d'apex d'une aile delta aux faibles vitesses. La Rech. Aéronaut. 74, 23–30.